Int J Earth Sci (Geol Rundsch) (2005) 94: 204–217
DOI 10.1007/s00531-005-0470-7

ORIGINAL PAPER

E. J. Catlos · Ibrahim Çemen

Monazite ages and the evolution of the Menderes Massif, western Turkey

Received: 1 September 2003 / Accepted: 11 December 2004 / Published online: 16 February 2005

Abstract The Menderes Massif experienced polyphase deformation, but distinguishing Pan-African events from Alpine tectono-metamorphic evolution, and discriminating Eocene–Oligocene shortening from recent extension remain controversial. To address this, monazite in garnet-bearing rocks from the massif's Gordes, Central, and Cine sections were dated in thin section (in situ) using the Th–Pb ion microprobe method. Cambro–Ordovician monazite inclusions in Cine and Central Menderes Massif garnets are ~450 m.y. older than matrix grains. Monazites in reaction with allanite from the Kuzey Detachment, which bounds the northern edge of the Central Menderes Massif, are 17 ± 5 Ma and 4.5 ± 1.0 Ma. The Pliocene result shows that dating of monazite can record the time of extension. The Kuzey Detachment might have exhumed rocks a lateral distance of ~53 km at a rapid rate of ~12 mm/year assuming the present ~20° ramp dip, Pliocene monazite crystallization at ~450°C, and a geothermal gradient of ~25°C/km. Assuming an angle of 60°, the rate decreases to ~5 mm/year, with the detachment surface at ~21 km depth in the Pliocene. Two Gordes Massif monazites show a similar allanite–monazite reaction relationship and are 29.6 ± 1.1 Ma and 27.9 ± 1.0 Ma, suggesting that the Cenozoic extension in the Gordes Massif, and possibly the entire Menderes Massif, might have begun in the Late Oligocene.

Keywords Monazite · Menderes Massif · Western Turkey · Geochronology · Extensional tectonics

E. J. Catlos (✉) · I. Çemen
School of Geology, Oklahoma State University,
105 NRC, Stillwater, OK 74078, USA
E-mail: catlos@okstate.edu
Tel.: +1-405-7449246
Fax: +1-405-7447841
E-mail: icmen@okstate.edu

Introduction

The Aegean extensional region (Fig. 1) experienced a series of continental collisions from Late Cretaceous to Eocene time, as evidenced by the Izmir-Ankara Neo-Tethyan suture zone (e.g., Sengor and Yilmaz 1981; Stampfli 2000). The collision zone may have trended southwestward, possibly close to the present position of the Hellenic arc (e.g., Doglioni et al. 1999). Post-collisional extension in the region, although controversial in its timing and nature, caused the exhumation of several Alpine metamorphic belts, termed the Menderes, Crete, Cyladic, Rhodope and Kazdag Massifs (Fig. 1). The largest of these, the Menderes Massif, accommodated significant extension and covers an area of >40,000 km^2 between the Izmir-Ankara Neo-Tethyan suture in the north and the Lycian Nappes to the south (Figs. 1, 2, 3).

Extension in the Aegean region might have been caused by: (1) tectonic escape and lateral extrusion, in which the Anatolian plate moves westward along the North and East Anatolian Faults (Fig. 1) in response to the collision of the Arabia and Eurasia (Sengor and Yilmaz 1981; Sengor et al. 1985; Cemen et al. 1999), (2) back-arc spreading due to the subduction along the Hellenic Arc (Fig. 1) (LePichon and Angelier 1979, 1981; Meulenkamp et al. 1988), or (3) orogenic collapse of thermally weakened lithosphere that experienced Paleogene contraction (Dewey 1988; Seyitoglu and Scott 1996). These hypotheses can be tested using geochronology, making the Menderes Massif a key locale in identifying the fundamental plate tectonic processes that facilitate extension in the continental lithosphere.

Central to our understanding of the development of the Menderes Massif, its exhumation history, and its relationship to broader tectonic events, is timing the transition from Alpine contraction to the extension now experienced by the region. Previous attempts to obtain the metamorphic history of the region include U–Pb and $^{207}Pb/^{206}Pb$ single zircon isotope dilution (Reischmann et al. 1991; Hetzel and Reischmann 1996; Hetzel et al.

1998; Loos and Reischmann 1999), K–Ar and $^{40}Ar/^{39}Ar$ biotite, muscovite, and amphibole (Seyitoglu and Scott 1992; Hetzel et al. 1995a, 1996; Gessner et al. 2001; Lips et al. 2001), Rb–Sr whole rock and mica (Satir and Friedrichsen 1986; Bozkurt and Satir 1999) and apatite and zircon fission track geochronology (Gessner et al. 2001). However, the age for initiation of Cenozoic extension in the Menderes Massif remains controversial.

In this paper, we present an alternative method to obtain the metamorphic history of the Menderes Massif: in situ ion microprobe monazite geochronology. Monazite, a rare earth phosphate mineral, is present in garnet-bearing rocks in the Menderes Massif. The mineral contains large amounts of Th and radiogenic Pb (e.g., Overstreet 1967), has a high ($>700°C$) closure temperature (e.g., Cherniak et al. 2004), and inclusions in garnet are shielded from Pb loss (e.g., Montel et al. 2000). The technique used here to date monazite (Catlos et al. 2002) preserves the grain and rock fabric, allowing for a clearer interpretation of the age. As part of a reconnaissance sampling survey, eight rocks were collected from the Menderes Massif. Samples 01-131 and 01-141 are from the Cine Massif; samples 01-88 and 01-127 are from the Central Menderes Metamorphic Core Complex; and samples 59-19-124b, 30, 01-26, and 01-13 are from the Gordes Massif (Fig. 2; Table 1).

Overall, 34 mineral grains were dated in situ. Of these, nine are inclusions in garnet. To help decipher the meaning of the monazite ages, X-ray element maps of garnets were collected using an electron microprobe and qualitatively evaluated. Monazite ages have provided information about the contractional history of regions (e.g., Harrison et al. 1997), but this paper presents the first data that monazite dated in garnet-bearing assemblages can provide information about an extensional history as well.

General geologic background

The Menderes Massif is divided into northern (Gordes), central, and southern (Cine) sections bounded by east-trending grabens, the Alasehir (Gediz) to the north and the Buyuk Menderes to the south (Figs. 2, 3) (see Bozkurt and Oberhaensli 2001). Rocks of the Menderes Massif consist of a lower unit, the ''core rocks'' of Cambro–Ordovician age (Sengor et al. 1984; Satir and Friedrichsen 1986; Loos and Reischmann 1999), and an upper unit of Paleozoic schist and Mesozoic–Cenozoic marble considered ''cover rocks'' (e.g., Sengor and Yilmaz 1981). Recently, several workers disputed this traditional ''core-cover'' interpretation (e.g., Ring et al. 1999; Gessner et al. 2001; Isik and Tekeli 2001).

For example, Fig. 3 shows a cross section through the Menderes Massif after Gessner et al. (2001). The Bayindir and Bozdag nappes consist of a metapelitic assemblage with amphibolite and marble lenses. Overlying the Bayindir and Bozdag nappes is

Fig. 1 Generalized map of the Aegean Region showing the location of Alpine Metamorphic belts and major structural elements

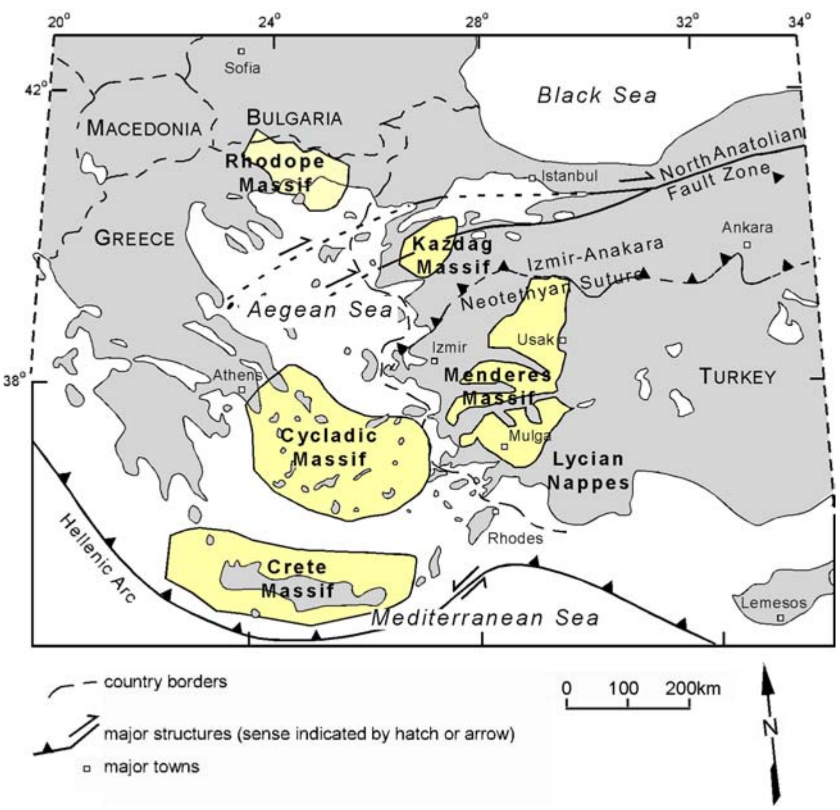

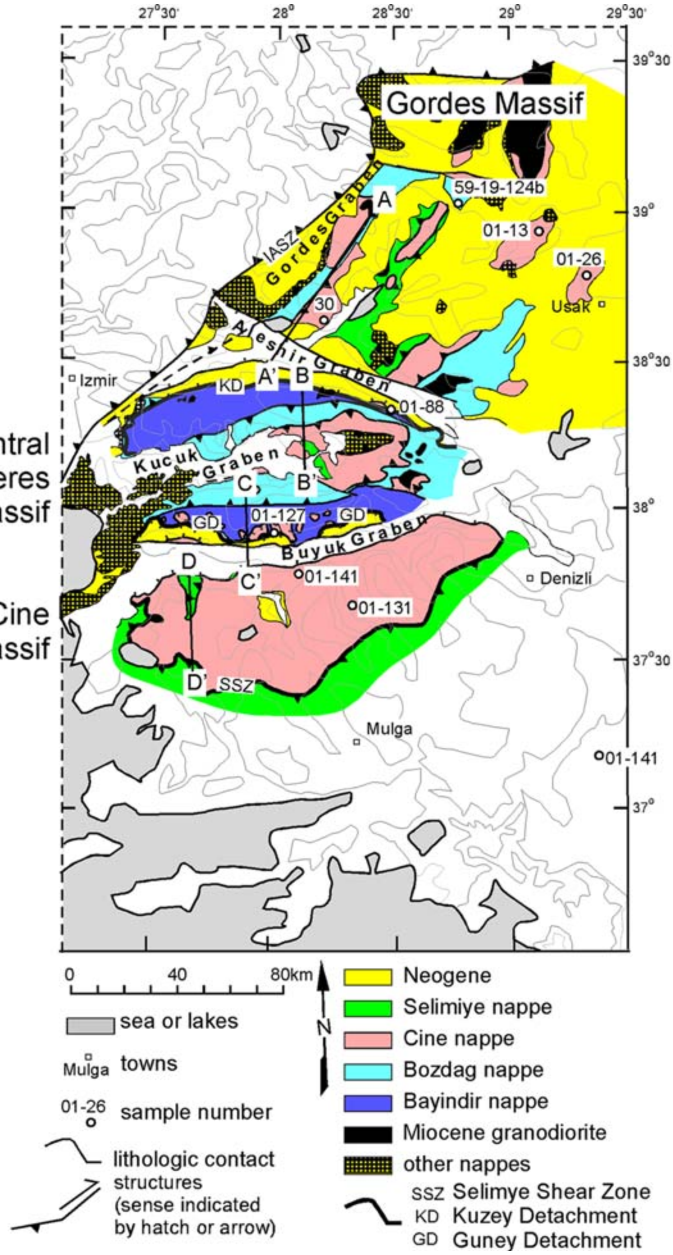

Fig. 2 Geologic map of the Menderes Massif (Gessner et al. 2001) with sample locations indicated. The Massif is divided into Gordes central, and Cine sections based on the presence of E–W trending grabens, the Alasehir Graben, Kucuk Menderes Graben, and Buyuk Menderes Graben. The Gordes region is characterized by roughly N–S trending grabens; we have only labeled the Gordes Graben. *KD* Kuzey Detachment, *GD* Guney Detachment, *SSZ* Selimiye Shear Zone. Cross-section lines from *A*–*D* correspond to Gessner et al. (2001)

Proterozoic–Cambrian basement assigned to the Cine nappe and an upper metasedimentary succession of intercalated marble and calcschist termed the Selimiye nappe. The Bayindir nappe might have experienced only one major Alpine tectonometamorphic event, whereas the overlying Bozdag, Cine and Selimiye nappes record both pre-Alpine and Alpine events (Ring et al. 1999).

The Central Menderes Metamorphic Core Complex is bounded by two detachments: (1) the north-dipping (10–20°N) Kuzey detachment (e.g., Hetzel et al. 1995a,

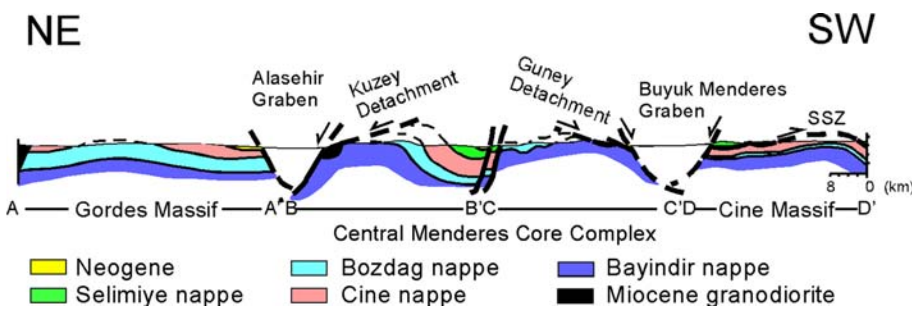

Fig. 3 Cross-section across the Menderes Massif (after Gessner et al. 2001). See Fig. 2 for lines of section

Table 1 Mineral assemblages and locations of the rocks analyzed

Sample	Latitude	Longitude	Assemblage											
	N	E	grt	bio	ms	chl	plg	ilm	zr	mnz	qtz	aln	xno	apt
Cine Massif														
01-131	37 41 43	28 19 35	a	a	a	a	a	a	a	a	a	a		
01-141	37 43 05	28 04 41	a	a	a	a	a	a	a	a	a			
Central Menderes Massif														
01-88	38 24 45	28 29 10	a	a	a	a	a	a	a	a	a	a	a	
01-127	37 53 38	28 06 23	a	a		a	a	a	a	a	a	a		
Gordes Massif														
59-19-124b	39 03 20	28 47 25	a	a	a	a	a	a	a	a	a			
01-26	38 46 40	29 24 35	a	a	a	a	a	a	a	a	a			a
30	38 40 23	28 14 10	a	a	a		a	a	a	a	a	a		a
01-13	38 55 15	29 05 30	a	a	a		a	a	a		a	a		a

grt garnet, *bio* biotite, *ms* muscovite, *chl* chlorite, *plg* plagioclase, *ilm* ilmenite, *zr* zircon, *mnz* monazite, *qtz* quartz, *aln* allanite, *xno* xenotime, *apt* apatite
[a]Mineral is found in the sample

b) and (2) the south-dipping (5–15°S) Guney detachment (e.g., Emre and Sozbilir 1997) (Figs. 2, 3). These structures cut upper levels of the nappe pile for an along-strike distance of 80 km and dip beneath the Alasehir and Buyuk Menderes Grabens, respectively (Fig. 3). Gessner et al. (2001) and Hetzel et al. (1995b) report an overall dome-shaped foliation pattern and north-northeast-trending stretching lineation in the Central Menderes Metamorphic Core Complex. They interpret the asymmetry of shear bands and quartz *c*-axis fabrics on either side of the structural dome to record top-to-the-north-northeast shear along the Kuzey detachment and top-to-the-north and to-the-south-southwest shear senses along the Guney detachment. The two opposite-dipping detachments with opposite senses of shear led to the proposal of a bivergent-rolling hinge model for the evolution of the Central Menderes Metamorphic Core Complex (Gessner et al. 2001).

Ion microprobe monazite geochronology

Background

Monazite, (Ce,La,Th)PO_4, occurs in pelites and granitoids as an accessory phase. Because of its capability to incorporate U and Th (e.g., Overstreet 1967) while avoiding significant amounts of Pb during crystallization, the mineral was an early candidate as a U–Th–Pb geochronometer (see Harrison et al. 2002). Despite its propensity for incorporating significant amounts of radioactive elements, monazite sustains little radiation damage (e.g., Meldrum et al. 1998) and has even been considered as a repository for nuclear waste (e.g., Ewing and LuMin 2002). According to Cherniak et al. (2004), monazite is impervious to Pb loss at high crustal temperatures (>700°C) and the ages reported here would not be affected by daughter product loss due to diffusion.

Monazite formation in pelites appears to vary as a function of bulk-rock composition and pressure–temperature (*P–T*) conditions (see Wing et al. 2003; Kohn and Malloy 2004). Precursor minerals in prograde metamorphic rocks are allanite, apatite, rare earth element (REE)- and Th-oxides (e.g., Smith and Barreiro 1990; Kingsbury et al. 1993). Along the retrograde path, monazite can replace allanite (Pan 1997; Finger et al. 1998) or pre-existing monazite (e.g., Ayers et al. 1999; Townsend et al. 2000).

Monazite inclusions in garnet are protected from daughter product loss (e.g., Foster et al. 2000; Montel et al. 2000; Catlos et al. 2001), whereas matrix grains can be exposed to retrograde fluids or subsequent reactions. These processes that take place after the grain crystallized affect its age and can be identified by statistical analyses. Samples with ages inconsistent with a single population have a mean square weighted deviation (MSWD) greater than 1. Catlos et al. (2002) outline the sources of uncertainty that can lead to this scenario, which include the growth of monazite along the retrograde path or during subsequent metamorphic episodes. Zoned monazite grains may have different age domains or individual single-grains can grow at different times within the sample.

Dating monazite using an in situ method is clearly warranted for rocks that experienced a complicated metamorphic history, as the monazite grain itself and its textural context is preserved. In addition, the *P–T* conditions estimated using the compositions of garnet and matrix minerals are commonly used with monazite age data to ascertain the evolution of metamorphic terranes (DeWolf et al. 1993; Harrison et al. 1997; Foster et al. 2000; Terry et al. 2000; Catlos et al. 2001). In this paper, we use the garnet-zoning patterns to help to qualitatively decipher the thermobarometric history of the sample.

Methods

Harrison et al. (1995) describe the method for monazite geochronology using an ion microprobe, which is briefly summarized here. An ion microprobe oxygen beam with a ~30-μm diameter is used to sputter isotopes of Th and Pb from monazite. An aperture window is used constrict the beam to a square shape. This is an important part of in situ analyses, as it eliminates the contamination from

Table 2 Monazite age data from Cine Massif sample 01-141

Grain-spot[a]	Location[b]	Th–Pb age (±1σ) (Ma)	ThO_2^+ /Th^{+c}	%^{207}Pb*d (±1σ)	208Pb*/Th^{+e} (±1σ)
11-1	i	571 (9)	2.395 (0.010)	74.2 (0.6)	2.867E-02 (4.544E-04)
9-1	i	488 (9)	2.379 (0.008)	78.3 (0.8)	2.446E-02 (4.497E-04)
10-1	i	437 (28)	2.696 (0.017)	37.8 (1.4)	2.186E-02 (1.398E-03)
12-1	m	44.7 (6.1)	2.264 (0.011)	18.5 (2.5)	2.214E-03 (3.007E-04)
3-1	m	47.1 (6.3)	1.779 (0.030)	21.5 (2.4)	2.334E-03 (3.127E-04)
2-1	m	42.8 (3.6)	1.991 (0.010)	35.5 (2.8)	2.122E-03 (1.796E-04)
1-1	m	33.1 (0.7)	2.643 (0.006)	62.6 (1.2)	1.637E-03 (3.698E-05)
01-141 calibration: $y=(0.078\pm0.002)x+1.196\pm0.045$, $r^2=0.988$, $ThO_2^+/Th^+=2.729\pm0.014$[f]					

[a]Nomenclature indicates the grain and spot, respectively, of the analyzed monazite. See Fig. 5 for BSE images of the grains
[b]Monazite inclusion in garnet is designated as "i", whereas "m" indicates a matrix grain
[c]Measured ratio in sample. Ideally, the ThO_2^+/Th^+ lies within the range defined by the standard monazite
[d]Percent radiogenically derived ^{207}Pb
[e]Corrected sample ratio assuming $^{207}Pb/^{204}Pb=39.5\pm0.1$ (Stacey and Kramers 1975)
[f]Calibration information: sample name, best fit of the calibration to the equation of a line (slope*x + intercept) with ±1σ uncertainty, correlation (r^2), and range of ThO_2^+ /Th^+ (±1σ) measured using monazite 554. Ideally, the unknown ThO_2^+ /Th^+ lies within the ThO_2^+/Th^+ range defined by the standard

common Pb contained in surrounding grains. Most of the monazite grains dated in this paper are ~20–40 μm, and no attempt was made to date specific chemical zones within the monazite itself. The mineral's composition may vary because of several factors, including crystal orientation, the transfer of elements from the breakdown of REE rich phases under changing P–T conditions, competitive crystallization among other REE phases in the rock, or replacement or recrystallization of an original grain during metamorphism (e.g., Cressey et al. 1999; Pyle and Spear 1999; Zhu and O'Nions 1999; Townsend et al. 2000).

The age standard used for the ion microprobe analyses was monazite 554, itself dated by isotope dilution (Force 1997). Several spots were analyzed on monazite 554, which created a line in ThO_2/Th versus ^{208}Pb/Th space (see Harrison et al. 1995; Catlos et al. 2002 for examples). The precision of the ages is limited by the reproduction of this calibration curve, which in this study had regression (r^2) values of 0.988 or 0.994, depending on analysis session (Tables 2, 3, 4). Some of the most uncertain results had ThO_2/Th values that did not lie within the range defined by the calibration curve (e.g., grain 3-1 in sample 01-141) (Table 2). In general, uncertainty is ±2% for Th–Pb ages (see also Harrison et al. 1995; Stern and Sanborn 1998; Harrison et al. 1999; Stern and Berman 2000). The uncertainty of all monazite and zircon ages reported here is 1σ.

For one Gordes Massif sample (01-13) monazite was not found, so we dated zircon in situ using the ion microprobe. To conduct these analyses, an oxygen beam with a ~30-*mu*m diameter is used to sputter isotopes of Pb only from the sample. No standards or calibration were used as we report only the $^{207}Pb/^{206}Pb$ ages (Table 5).

Table 3 Monazite age data from Central Menderes Massif samples

Grain-spot[a]	Location[b]	Th–Pb age (±1σ) (Ma)	ThO_2^+/Th^{+c} (±1σ)	%^{207}Pb*d (±1σ)	208Pb*/Th^{+e} (±1σ)
01-88					
1-1	i	512 (9)	2.594 (0.022)	98.0 (0.6)	2.564E-02 (4.696E-04)
5-1	i	483 (5)	2.746 (0.016)	99.3 (0.1)	2.420E-02 (2.368E-04)
9-1	m	17 (5)	2.399 (0.012)	8.3 (2.5)	8.353E-04 (2.459E-04)
3-1	m	4.5 (1.0)	2.437 (0.008)	21.8 (4.4)	2.241E-04 (4.801E-05)
01-88 calibration: $y=(0.078\pm0.002)x+1.196\pm0.045$, $r^2=0.988$, $ThO_2^+/Th^+=2.729\pm0.014$[f]					
01-127					
8-1	m	563 (7)	3.266 (0.014)	99.7 (0.03)	2.826E-02 (3.545E-04)
8-2	m	496 (4)	3.563 (0.013)	99.7 (0.03)	2.483E-02 (2.192E-04)
8-3	m	414 (6)	3.225 (0.019)	99.7 (0.04)	2.067E-02 (3.175E-04)
7-1	m	536 (5)	3.694 (0.019)	99.6 (0.04)	2.689E-02 (2.786E-04)
4-1	m	503 (7)	3.983 (0.019)	99.5 (0.07)	2.517E-02 (3.564E-04)
01-127 calibration: $y=(0.115\pm0.007)x+1.240\pm0.143$, $r^2=0.994$, $ThO_2^+/Th^+=3.606\pm0.015$[f]					

[a]Nomenclature indicates the grain and spot of the analyzed monazite. See Fig. 8 for BSE images of grains from sample 01-88
[b]Monazite inclusion in garnet is designated as "i", whereas "m" indicates a matrix grain
[c]Measured ratio in sample. Ideally, the ThO_2^+/Th^+ lies within the range defined by the standard monazite
[d]Percent radiogenically derived ^{207}Pb
[e]Corrected sample ratio assuming $^{207}Pb/^{204}Pb=39.5\pm0.1$ (Stacey and Kramers 1975)
[f]Calibration information: sample name, best fit of the calibration to the equation of a line (slope*x + intercept) with ±1σ uncertainty, correlation (r^2), and range of ThO_2^+/Th^+ (±1σ) measured using monazite 554. Ideally, the unknown ThO_2^+/Th^+ lies within the ThO_2^+/Th^+ range defined by the standard

Table 4 Monazite age data from Gordes Massif samples

Grain-spot[a]	Location[b]	Th–Pb age (±1σ) (Ma)	ThO_2^+/Th^{+c} (±1σ)	$\%^{207}Pb^*d$ (±1σ)	$208Pb^*/Th^{+e}$ (±1σ)
59-19-124b					
4-1	i	39.7 (0.9)	3.339 (0.020)	95.1 (1.0)	1.966E-03 (4.488E-05)
5-1	i	37.9 (1.1)	3.047 (0.023)	96.5 (0.6)	1.877E-03 (5.406E-05)
3-1	i	36.1 (0.8)	3.447 (0.034)	95.7 (0.7)	1.788E-03 (4.033E-05)
1-1	m	32.8 (0.5)	3.864 (0.020)	96.8 (0.5)	1.625E-03 (2.286E-05)
01-26					
1_1	i	36.0 (0.6)	4.130 (0.011)	96.8 (0.5)	1.784E-03 (3.170E-05)
3_2	m	41.4 (1.3)	3.007 (0.013)	92.4 (0.9)	2.050E-03 (6.568E-05)
2_1	m	38.4 (0.8)	3.499 (0.048)	92.3 (1.0)	1.903E-03 (4.086E-05)
3_1	m	33.6 (0.7)	3.873 (0.023)	90.9 (1.2)	1.664E-03 (3.356E-05)
5_1	m	33.6 (0.8)	3.364 (0.007)	95.8 (0.6)	1.662E-03 (3.879E-05)
5_1	m	33.0 (0.5)	2.487 (0.006)	91.5 (0.9)	1.444E-03 (1.685E0–5)
4_1	m	29.6 (1.1)	3.416 (0.021)	74.5 (2.4)	1.463E-03 (5.458E-05)
6_2	m	29.2 (0.3)	2.913 (0.006)	91.8 (0.7)	1.444E-03 (1.685E-05)
6_1	m	28.2 (0.4)	2.814 (0.009)	86.9 (0.9)	1.398E-03 (1.806E-05)
30					
5_1	m	52.9 (5.7)	2.395 (0.016)	88.2 (1.4)	2.619E-03 (2.823E-04)
4_1	m	43.2 (3.6)	2.558 (0.019)	91.0 (1.1)	2.140E-03 (1.767E-04)
2_1	m	42.7 (0.9)	3.453 (0.010)	93.4 (0.7)	2.116E-03 (4.318E-05)
3_1	m	41.4 (1.7)	3.007 (0.010)	94.2 (0.7)	2.050E-03 (8.273E-05)
1_1	m	40.1 (0.9)	3.400 (0.011)	96.0 (0.8)	1.985E-03 (4.534E-05)
6_3	m	35.1 (0.3)	2.424 (0.005)	93.5 (0.4)	1.739E-03 (1.702E-05)
5_2	m	27.9 (1.0)	4.824 (0.058)	75.9 (1.7)	1.380E-03 (4.880E-05)
6_2	m	26.9 (0.6)	4.420 (0.015)	86.4 (0.9)	1.330E-03 (3.114E-05)

Calibration: $y = (0.078 \pm 0.002)x + 1.196 \pm 0.045$, $r^2 = 0.988$, $ThO_2^+/Th^+ = 2.729 \pm 0.014$[f]

[a]Nomenclature indicates the grain and spot, respectively, of the analyzed monazite. See Figs. 9 and 10, for BSE images of these samples
[b]Monazite inclusion in garnet is designated as "i", whereas "m" indicates a matrix grain
[c]Measured ratio in sample. Ideally, the ThO_2^+/Th^+ lies within the range defined by the standard monazite
[d]Percent radiogenically derived ^{207}Pb
[e]Corrected sample ratio assuming $^{207}Pb/^{204}Pb = 39.5 \pm 0.1$ (Stacey and Kramers 1975)
[f]Calibration information for all Gordes Massif samples, best fit of the calibration to the equation of a line (slope*x + intercept) with $\pm 1\sigma$uncertainty, correlation (r^2), and range of ThO_2^+/Th^+ ($\pm 1\sigma$) measured using monazite 554. Ideally, the unknown ThO_2^+/Th^+ lies within the ThO_2^+/Th^+ range defined by the standard

Applications

An ideal application of monazite geochronology is to the understanding compressional orogens with a simple one-stage metamorphic history. For example, Fig. 4 shows schematic P–T diagrams for allanite (Catlos et al. 2002), loosely based on the epidote stability field (e.g., Liou 1973) and observations of the relationship of allanite and monazite in metamorphic rocks (e.g., Overstreet 1967). Because allanite has the potential to accept more elements than epidote, Catlos et al. (2002) speculate that allanite is able to exist over a wider range of pressure and temperature conditions. Along the prograde P–T path in Fig. 4a, monazite grows via allanite breakdown; whereas, along the retrograde path, monazite is affected by subsequent fluid-mediated reactions (e.g., Ayers et al. 1999). Townsend et al. (2000) suggests that these retrograde reactions can occur at temperature as low as 450°C.

In Fig. 4b, we propose another mechanism in which monazite can appear, in which a rock crosses from the allanite to monazite stability field during decompression. The composition of the allanite exerts a major control on the boundaries of its stability field. Therefore, a rock following this P–T path may have monazite ages inconsistent with a single population, as the conditions in which monazite would precipitate depends on the composition of the allanite reactant. This P–T path scenario suggests that in situ monazite dating method could be applied to understand the timing of extension, including slip along the Kuzey and Guney detachments in the Menderes Massif.

Table 5 Matrix zircon age data from Gordes Massif sample 01-13

Grain_spot[a]	Age[b] (Ma) (±1σ)	$\%^{206}Pb^{*c}$ (±1σ)
5_1	558 (62)	96.8 (0.1)
4_1	499 (134)	98.5 (0.3)
3_1	493 (79)	99.5 (0.2)
2_1	481 (78)	99.5 (0.2)

[a]Nomenclature indicates the grain and spot, respectively, of the analyzed zircon
[b]^{207}Pb–^{208}Pb ion microprobe zircon ages
[c]Percent radiogenically derived ^{206}Pb

Results

Cine Massif

In the Cine Massif (Fig. 2), $^{207}Pb/^{206}Pb$ single zircons and Rb–Sr whole rock data yield Cambro–Ordovician or older ages (Satir and Friedrichsen 1986; Hetzel and Reischmann 1996; Loos and Reischmann 1999). A ductile shear zone, termed the Selimiye Shear Zone forms the southern margin of the Cine Massif. Activity along the shear zone is syn- or pre-Eocene, based on Rb–Sr muscovite and biotite and $^{40}Ar/^{39}Ar$ muscovite ages (Satir and Friedrichsen 1986; Hetzel and Reischmann 1996; Lips et al. 2001).

Metamorphic grade within the Cine Massif appears to increase from south to north (Bozkurt 1996; Whitney and Bozkurt 2002; Regnier et al. 2003). Based on garnet element maps, mineral compositions, and thermobarometry, Whitney and Bozkurt (2002) suggest that the upper schists of the Cine Massif reached temperatures of ~425–550°C and experienced only one regional metamorphic event. Although some Cine Massif samples contain garnets of different sizes, they interpreted the variation to reflect a difference in the local environment of nucleation and growth rates, as smaller grains appeared in quartz-rich domains and larger grains are located in mica-rich layers. Regnier et al. (2003) found that Cine metasedimentary rocks located beneath the Selimiye Shear Zone record conditions of ~7 kbar and >550°C whereas Cine rocks ~20–30 km north record 8–11 kbar and 600–650°C.

We collected sample 01-141 from the Cine nappe (Fig. 2; Table 1) and obtained in situ ion microprobe Th–Pb ages of monazite inclusions in garnet and in the matrix (Fig. 5; Table 2). Most 01-141 garnets are fragmented, appear in retrograde reaction to chlorite and contain small grains of monazite and quartz, as well as veins of chlorite and quartz. Monazite inclusions in garnet yielded an average age of 501 ± 18 Ma (MSWD = 41), whereas matrix grains yielded an average age of 42 ± 5 Ma (MSWD = 53). The ages indicate that the Cine Massif sample 01-141 experienced at least a two-stage metamorphic history.

Monazites that yielded Cambro–Ordovician ages are found only as inclusions in garnet, whereas monazites

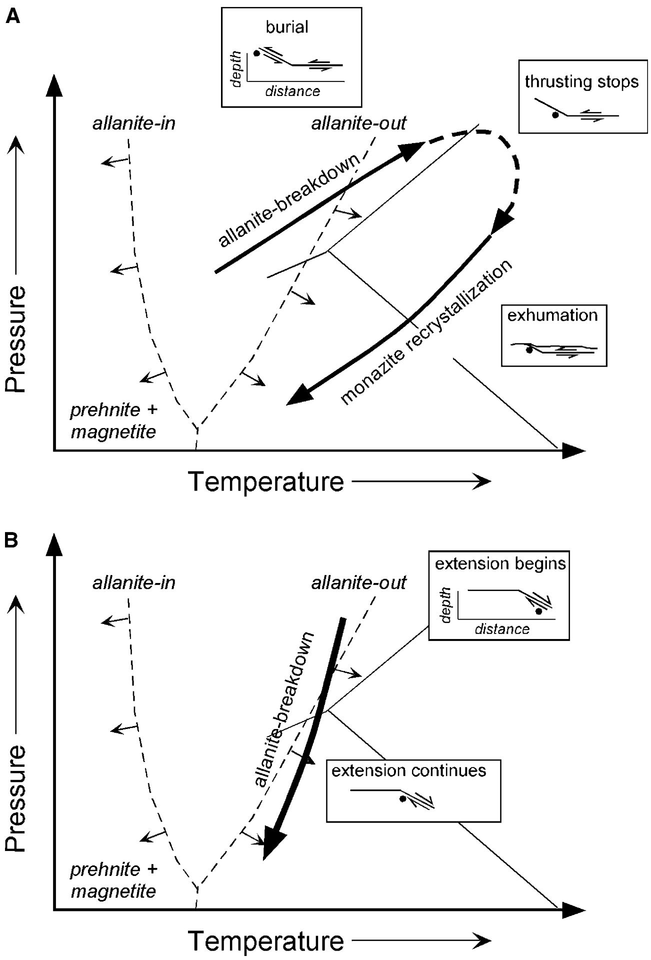

Fig. 4 a *P–T* diagram of allanite (after Catlos et al. 2002). Monazite may form along the prograde leg of the *P–T* path via allanite-break down reactions. *Insets* show a schematic evolution of a fictional sample (*black circle*) affected during compression. The sample is buried along the prograde path, subjected to high *T* as thrusting stops as heat is supplied across the ramp, and affected by retrograde reactions during exhumation. **b** In this scenario, monazite forms along the retrograde leg of the *P–T* path via allanite-break down reactions. *Insets* show a schematic evolution of a fictional sample affected during extension. The length and shape of the path is schematic

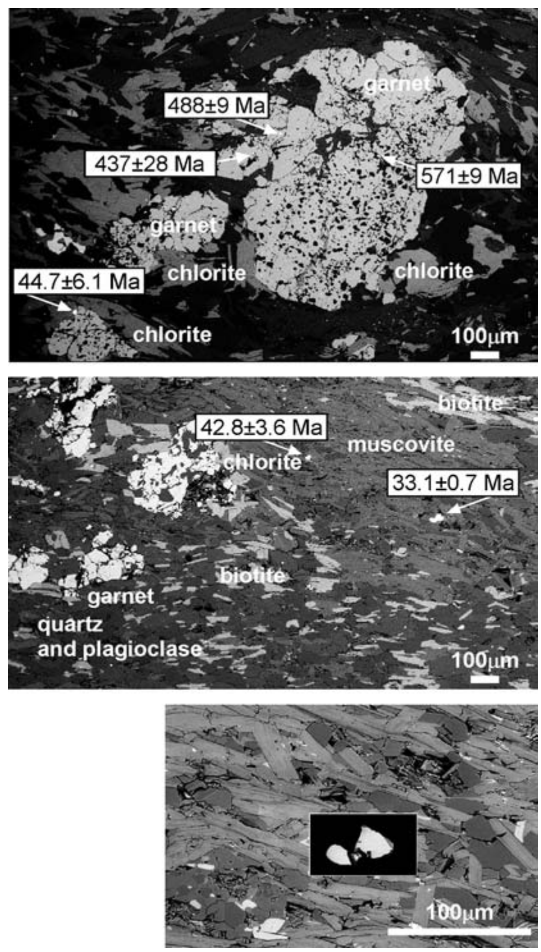

Fig. 5 Backscattered (BSE) electron images of Cine Massif sample 01-141 with Th–Pb monazite ages indicated with 1σ error. Other minerals present in the rock are labeled. The *lowest figure* is a high contrast BSE image of the 33.1 ± 0.7 Ma grain. See Table 2 for analysis details

that yield Eocene–Oligocene ages are found only in the matrix. The monazite grain in the core of the garnet is older than the rim monazites by 97–171 million years, taking into account the 1σ uncertainties (Fig. 5; Table 2). This textural relationship, combined with the observation that monazite inclusions in garnet are protected from Pb loss, suggest that 01-141 garnets might have grown during Pan-African deformation. Matrix grains were not shielded by the garnet from subsequent metamorphism or retrograde reactions and were the source material for monazite crystallization during the Eocene–Oligocene. This interpretation is based on the similarity in size and shape of the monazite grains in the garnet and in the matrix. The ages of monazite in the matrix are similar to $^{40}Ar/^{39}Ar$ muscovite ages from samples collected near the Selimiye Shear Zone (43.4 ± 1.3–37.9 ± 0.4 Ma; Hetzel and Reischmann 1996), suggesting a link between movement across the shear zone and matrix monazite crystallization in 01-141.

X-ray element maps of garnets in sample 01-131 collected from the Cine unit (Fig. 2; Table 1) also support the possibility that the Cine Massif experienced two stages of metamorphism (Fig. 6). X-ray Mn map of garnets in this sample show a discontinuous increase from mid-rim to rim that defines a broad (~30 μm) plateau. The increase appears at the same location as a sharp Ca decrease and Mg increase and is not found near minerals characteristic of retrogression (e.g., chlorite). The profile leaves open the possibilities that the garnets grew during two stages. Alternatively, the rock might have experienced a change in bulk composition during rim growth along a single P–T path. In any case, the sharp decrease in Ca combined with the presence of albitic plagioclase in this rock is consistent with decompression (Spear 1993).

The possibility of polymetamorphic garnet growth in the Cine Massif has implications for attempts to obtain peak P–T conditions from the region using garnet-based thermobarometric methods (e.g., Ashworth and Evirgen 1984, 1985; Whitney and Dilek 1998a, b; Whitney and Bozkurt 2002; Regnier et al. 2003). P–T conditions are used to evaluate models of the evolution of the Menderes Massif (Okay 2001; Ring et al. 2001; Whitney and Bozkurt 2002; Regnier et al. 2003). Sample 01-141 might have been affected by metamorphic events separated by ~450 m.y. Therefore, obtaining P–T conditions using compositions from this sample's garnet and matrix minerals would lead to a meaningless result. Microtectonic studies are useful for identifying pre-, inter-, syn-, and post-metamorphic garnet growth (e.g., Bozkurt 1996; Passchier and Trouw 1996; Regnier et al. 2003). Monazite in situ ion microprobe geochronology is an important addition to this technique that can be used to provide timing constraints on the episodes of deformation that might have affected the Cine Massif.

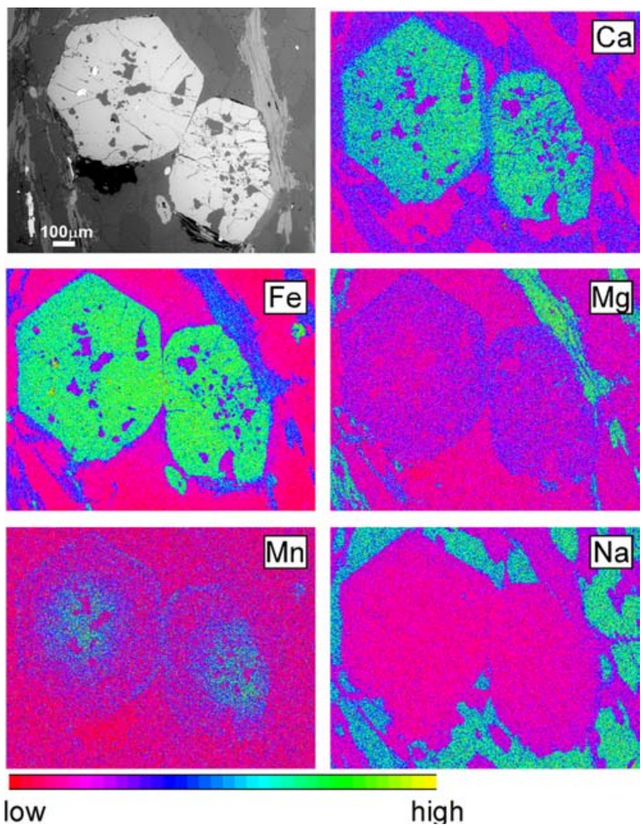

Fig. 6 BSE image (*upper left*) and X-ray element maps of Ca, Fe, Mg, Mn, and Na (*labeled*) of Cine Massif garnets from sample 01-131. Matrix minerals include biotite, quartz and plagioclase

Central Menderes Massif

Timing of slip across the north-dipping Kuzey and south-dipping Guney detachments has implications for understanding the exhumation history of the Central Menderes Metamorphic Core Complex (e.g., Lips et al. 2001). Hetzel et al. (1995a, b) proposed that extension began along the Kuzey detachment surface in early Miocene time based on the $^{40}Ar/^{39}Ar$ amphibole age of 19.5 ± 1.4 Ma from a syn-extensional granodiorite that intruded prior to brittle deformation along the detachment surface. However, the argon age spectrum and correlation diagram of the Kuzey detachment amphibole shows that the sample is affected by excess argon (Fig. 7). Despite this recognition, the isochron age of this amphibole is interpreted to reliably indicate the age of early Miocene extension (Gessner et al. 2001; Lips et al. 2001; Seyitoglu and Scott 1996). The extensional origin of the granodiorite is also controversial (Yilmaz et al. 2000). The granodiorite may be related to crustal thickening during deformation along the Izmir-Ankara suture zone. Such an interpretation would preclude an Early Miocene initiation age of extension in western Turkey.

Lips et al. (2001) step-heated handpicked grains of syn-kinematic muscovite collected from the Buyuk Menderes graben and Kuzey Detachment (Fig. 7). Their results of $^{40}Ar/^{39}Ar$ laser-probe experiments resulted in large analytical errors attributed to the analysis of small

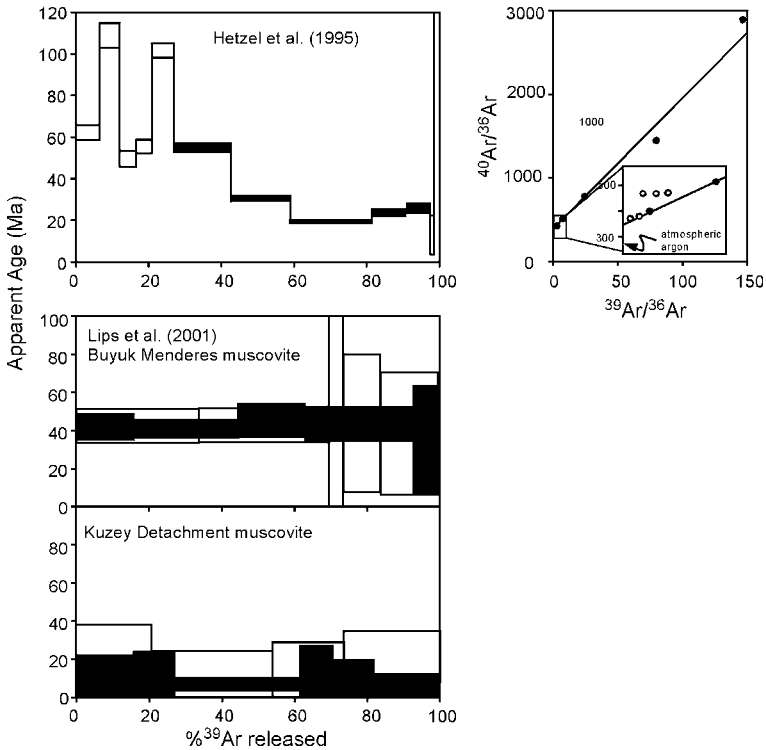

Fig. 7 Results of step-heated amphibole argon age spectra (*upper left*) and correlation diagram (*upper right*) after (Hetzel et al. 1995a). Note that the correlation isochron for this sample intersects ^{36}Ar/^{40}Ar values at a non-atmospheric value. Black steps (*left upper figure*) correlate to black circles (*right upper figure*), and were used to calculate the isochron age of 19.5 ± 1.4 Ma. *Lower* Results of ^{40}Ar/^{39}Ar laser-probe experiments of two muscovite samples from the Buyuk Menderes and two muscovite samples from the Kuzey Detachment (after Lips et al. 2001)

samples (< 0.2 mg), therefore low argon retentivities. Lips et al. (2001) report single fusion muscovite ages of 36 ± 2 Ma from the Buyuk Menderes graben and 7 ± 1 Ma from the Kuzey detachment. The Oligocene muscovite age is attributed to recrystallization of the deformational fabric, which was accompanied or followed by extensional ductile faulting along the southern margin of the Menderes Massif, whereas the Late Miocene age is attributed to the last stage of activity along the Kuzey detachment or to continuous movement across the low-angle fault zone.

We collected a sample from rocks along the Kuzey detachment (sample 01-88) (Figs. 2, 8; Table 1) and from the Guney detachment (sample 01-127) (Fig 2; Table 1) and obtained in situ ion microprobe Th–Pb ages for monazite inclusions in garnet and in the matrix (Table 3).

Garnets in 01-88 are rounded and contain inclusions of monazite and quartz. X-ray element maps indicate that these garnets are not zoned in Mn, Ca, Mg, or Fe. The 01-88 garnet contains monazites that yield Cambro–Ordovician average ages of 498 ± 7 Ma (MSWD = 11), whereas sample 01-127 contains monazites in the matrix that also yield Cambro-Ordovician average ages of 502 ± 6 Ma (MSWD = 85) (Table 3). The monazite inclusions in 01-88 garnets have a strikingly different shape compared to those in the matrix, which are only found in contact with allanite (Fig. 8). Inclusions in garnet are small and rounded, whereas matrix monazite appears to assume the shape of the allanite grains. The difference in the shapes suggests that the monazites in the garnet grew in an environment wholly different than those in the matrix, possibly in a completely different rock. This observation, along with the large difference in ages between the matrix and inclusion ages, suggests the 01-88 garnet may be detrital. Obtaining *P–T* conditions using garnet and matrix mineral compositions would lead to a meaningless result.

The textural relationship of the dated matrix grains suggests an allanite → monazite reaction, one that is typical of prograde metamorphic terranes (e.g., Smith and Barriero 1990). However, the age of 4.5 ± 1.0 Ma from one monazite grain is younger than any speculated Menderes Massif compressional event. The age is within 1σ of the apatite fission track result of 3.7 ± 0.6 Ma from a rock collected along the same detachment (Gessner et al. 2001). These results indicate that the Central Menderes Metamorphic Complex sample 01-88 has monazite grains that record extension.

Gordes Massif

Palynological ages of 20–14 Ma (Seyitoglu et al. 1994; Seyitoglu and Scott 1996) and K–Ar biotite ages of 16.9 ± 0.5–18.4 ± 0.8 Ma of igneous rocks from the Gordes Graben (Fig. 2) (Seyitoglu et al. 1994) are similar to the excess-argon affected 19.5 ± 1.4 Ma age from the potentially syn-extensional Kuzey detachment surface granodiorite (Hetzel et al. 1995a, b). The ages suggest E–W and N–S trending Menderes Massif grabens formed simultaneously in Early Miocene (Seyitoglu and Scott 1996).

In the Gordes Massif, sample 59-19-124b was collected from the Bozdag nappe whereas samples 30, 01-13, and 01-26 are from the Cine nappe (Fig. 2; Table 1). Monazite was not found in 01-13; we report ^{207}Pb/^{206}Pb

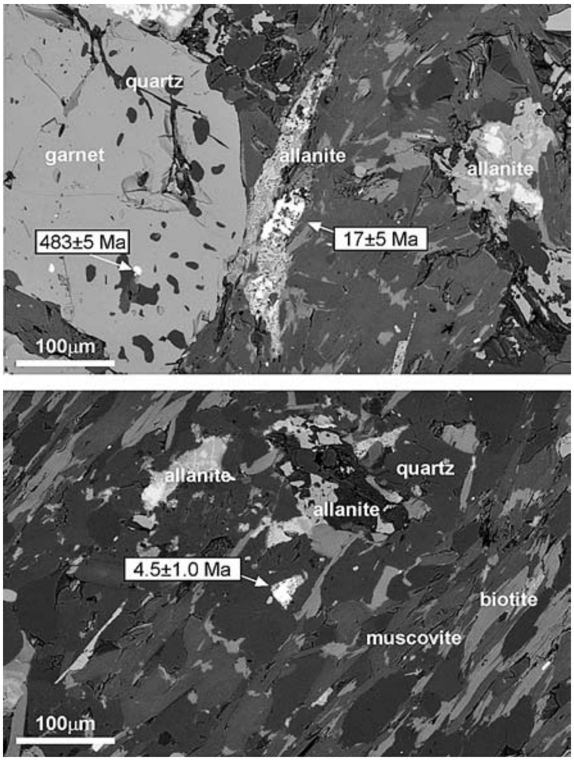

Fig. 8 BSE images of Central Menderes Metamorphic Core Complex sample 01-88 with Th–Pb monazite ages indicated with 1σ error. Upper image after (Harrison et al. 2002). Other minerals present in the rock are labeled. See Table 3 for analysis details

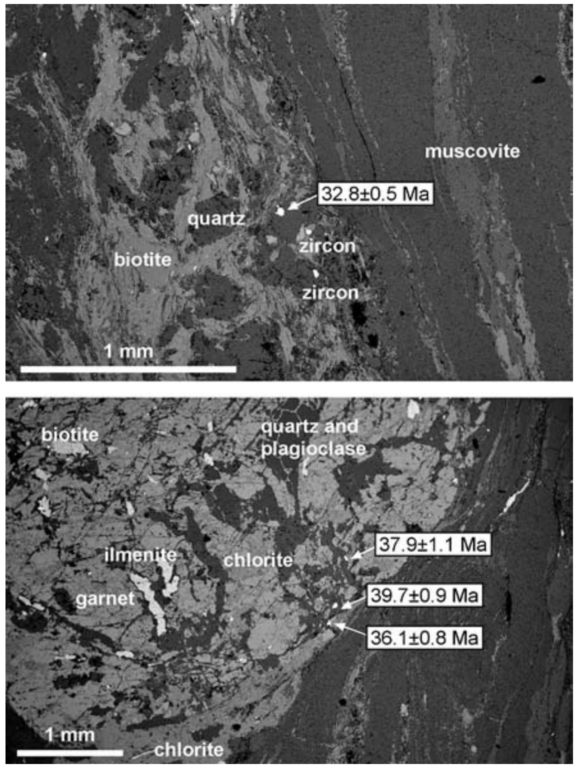

Fig. 9 BSE images of Gordes Massif sample 59-19-124b with Th–Pb monazite ages indicated with 1σ error. Other minerals present in the rock are labeled. See Table 4 for analysis details

ion microprobe zircon ages from this sample (Table 5), which average 508 ± 92 Ma (MSWD = 0.3) and are within 1σ of whole rock Rb–Sr ages of 471 ± 9 Ma (Satir and Friedrichsen 1986).

Garnets in sample 59-19-124b are retrogressed to chlorite and contain 39.6 ± 0.9–36.1 ± 9.8 Ma monazite inclusions that are 6–8 m.y. older than that in the matrix (Fig. 9; Table 4). The garnet in 59-19-124b might have shielded inclusions from Pb loss (e.g., Montel et al. 2000), whereas the matrix grain could have been exposed to alteration due to fluid-mediated retrograde reactions. We adopt this hypothesis as opposed to later crystallization during prograde metamorphism because of the textures shown by the garnet in sample 59-19-124b (Fig. 9).

The garnet in sample 01-26 is euhedral and contains inclusions of quartz, zircon, and monazite (Fig. 10). Quartz inclusions in the garnet core curve and the rim inclusions appear continuous with the external fabric, suggesting syntectonic growth. The 36.0 ± 0.6 Ma monazite inclusion in the 01-26 garnet is both older and younger than matrix grains (Table 4).

X-ray element maps of the garnet show no evidence of diffusion (Fig. 11), and therefore we cannot attribute the younger ages in the matrix of this rock to diffusive Pb loss (see also Cherniak et al. 2004). The maps suggest that the 36.0 ± 0.6 Ma-old monazite inclusion became incorporated into the garnet over a *P*–*T* path of increasing *T* and decreasing *P* (e.g., Spear 1993). The garnet began Mn-rich, became more Fe-rich until a maximum value was reached, and then Mg increased, consistent with growth under increasing *T*. The core of the garnet is more Ca-rich than the rim, and the plagioclase in the rock is albitic, consistent with growth over a decompression path.

Matrix grains in sample 01-26 record episodes of monazite growth and/or retrograde reactions. One monazite is in close reaction relationship with allanite and yields an age of 29.6 ± 1.1 Ma (Fig. 10). Based on the similar relationship present in sample 01-88, the possibility exists that this monazite age records monazite growth during extension. Overall, the ages from 01-26 (Table 4) are within range of those obtained from the Cine Massif (Table 2), indicating that the massif experienced monazite growth events throughout the Late Eocene to Early Oligocene time.

Monazite grains in sample 30 yield ages from 53 ± 6–26.9 ± 0.6 Ma (Fig. 12; Table 4). Oligocene to Miocene grains are within range of 24.0 ± 0.3 Ma and 35 ± 1 Ma Rb–Sr biotite ages (Satir and Friedrichsen 1986). Two spots on a monazite adjacent to allanite yield 53 ± 6 Ma and 27.9 ± 1.0 Ma (Fig. 12). The older age has larger uncertainty due to its position relative to the ion microprobe calibration and lower amounts of radiogenic Pb (Table 4). The younger spot is within 1σ of the 29.6 ± 1.1 Ma age of a monazite grain found in a similar textural relationship in sample 01-26, indicating the rocks experienced a synchronous allanite to monazite reaction. These observations, coupled with the Late

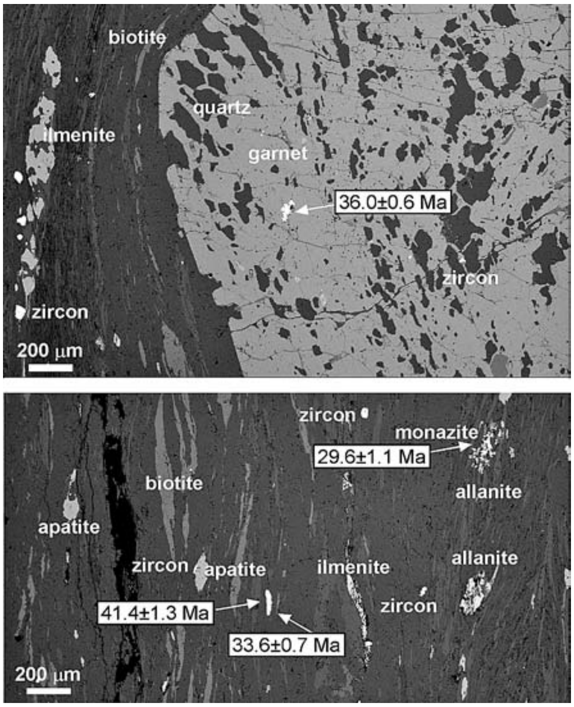

Fig. 10 BSE images of Gordes Massif sample 01-26 with Th–Pb monazite ages indicated with 1σerror. Other minerals present in the rock are labeled. See Table 4 for analysis details

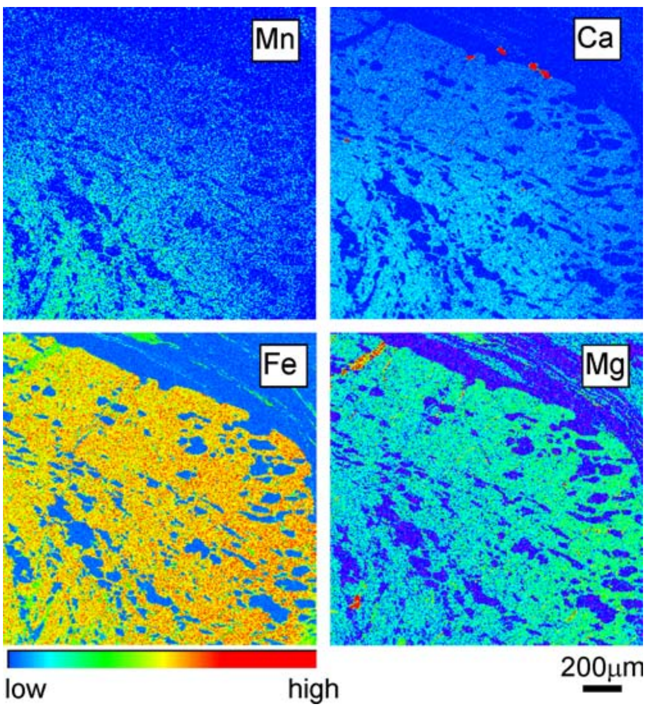

Fig. 11 X-ray element maps of Mn, Ca, Fe, and Mg from the Gordes Massif garnet 01-26 seen in Fig. 10. The garnet preserves its elemental distribution, indicating that the mineral did not experience significant diffusion

Miocene–Pliocene ages of monazites adjacent to allanite in 01-88, leave open the possibility that the reactions occurred during decompression and imply that the

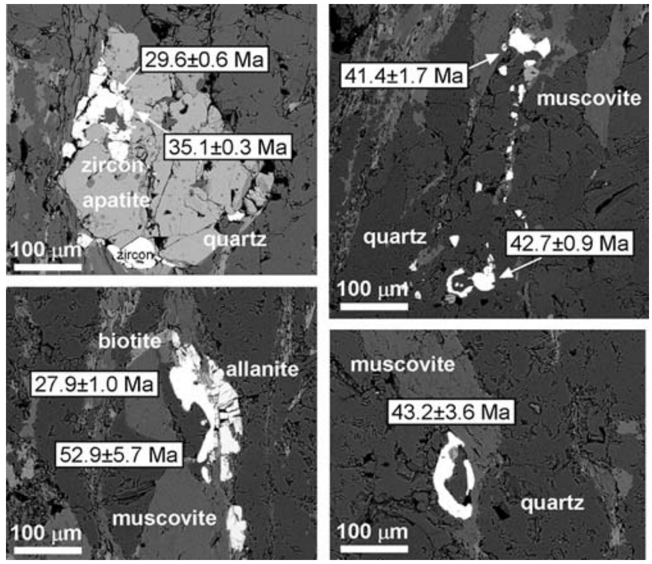

Fig. 12 BSE image of Menderes Massif sample 30 with Th–Pb monazite ages indicated ($\pm 1\sigma$). Other minerals present in the rock are labeled. See Table 4 for analysis details

Menderes Massif experienced extension during Oligocene time.

Discussion and conclusions

Monazite growth during decompression

Other than the Cambro–Ordovician ages, monazite ages from the Menderes Massif range from 53 ± 6 Ma to 4.5 ± 1.0 Ma. If all Cenozoic monazite grains formed during decompression, extension in the Menderes Massif might have begun in the Eocene time. Whether the monazites grew during compression, decompression due to detachment faulting or erosional exhumation remains in question.

However, monazite can effectively record ages related to tectonically controlled extension. Sample 01-88, collected from the Kuzey Detachment, contains a 4.5 ± 1.0 Ma-old matrix grain (Fig. 8), which is inconsistent with any previous geochronologic constraints connected with compression. The structural location of the sample and similar zircon and apatite fission track results reported from the same detachment elsewhere (Gessner et al. 2001) are consistent with the idea that the matrix monazite in this rock formed due to allanite breakdown reactions during extension. The 4.5 ± 1.0 Ma and 17 ± 5 Ma monazite grains show the same textural relationships to allanite, and movement along the Kuzey Detachment might have begun during the early Miocene and continued in the Pliocene.

Figure 4b illustrates how we envision that monazite formed in sample 01-88. The rock was initially within the allanite stability field when extension initiated. Allanite with a suitable chemical composition reacted

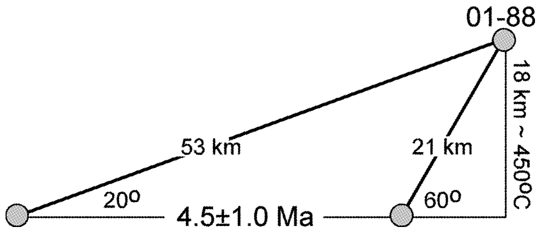

Fig. 13 Schematic calculations of how the younger monazite in sample 01-88 (*grey circle*) could have been transported to the surface along a 20° or 60° detachment surface

to form monazite due to decompression under different *P–T* conditions at 17 ± 5 Ma and 4.5 ± 1.0 Ma. These *P–T* conditions are currently unknown. However, assuming monazite crystallization at ~4.5 Ma at ~450°C (Townsend et al. 2000), a ~20° ramp on the Kuzey Detachment (Hetzel et al. 1995a), and a geothermal gradient of ~25°C/km, the Pliocene monazite age suggests the Kuzey Detachment exhumed a lateral distance of ~53 km at a rate of ~12 mm/year since the Pliocene (Fig. 13). Alternatively, the Kuzey detachment might have initially formed as a high-angle normal fault at depth and then became a low-angle detachment surface due to flexural rotation/rolling hinge processes (Seyitoglu et al. 2000, 2002). If the initial dip of the Kuzey Detachment was ~60°, the Pliocene monazite age constrains the movement to ~5 mm/year, exhuming ~21 km (Fig. 13).

Because significant gaps exist in our understanding of the conditions of monazite formation, many variables in these calculations are speculative. The rates and distances calculated use only the younger monazite in 01-88, and are complicated by the presence of the 17 ± 5 Ma grain. Both monazites show the same textural relationships to allanite and movement along the Kuzey Detachment might have initiated during the Miocene. Support for this hypothesis, as well as a better understanding of the meaning of the monazite ages, requires further examination before the ages are conclusively applied to understand the slip history of the Kuzey Detachment.

Pan-African monazite inclusions in garnet

The Pan-African history of the Menderes Massif is an important constraint for Pangean reconstructions. The southeast European Alpine and Mediterranean mountain belts contain zircons that yield Pan-African ages (e.g., Neubauer 2002) and the Menderes Massif exposes a wide area of rocks that record this late Neoproterozoic to early Paleozoic event (Satir and Friedrichsen 1986; Loos and Reischmann 1999; Oelsner et al. 1997). Therefore, the region provides an important locale for making paleogeographic reconstructions (Sengor et al. 1984; Neubauer 2002). In situ dating of monazite inclusions in garnet has the potential to yield information about the duration and nature of Pan-African deformation (Oelsner et al. 1997).

Monazite ages are important for deciphering the origin of garnets found in the Menderes Massif. Garnet-based *P–T* conditions are frequently used to evaluate and develop models for the tectonic evolution of the Menderes Massif (e.g., Okay 2001; Ring et al. 2001). If the garnets are detrital, as speculated for 01-88, or developed during to a previous Pan-African related metamorphic event, as speculated for 01-141, using their compositions in combination with the matrix minerals would generate misleading thermobarometric conditions and erroneously constrained tectonic models.

Implications for extensional tectonics in the Menderes Massif

Mechanisms responsible for extension in west Anatolia remain poorly understood and likewise the beginning of extension remains poorly documented. In this paper, we suggest the possibility that extension in Gordes Massif occurred in Late Oligocene time based on the 29.6 ± 1.1 Ma-old and 27.9 ± 1.0 Ma-old monazite grains (Table 4) that have textural relationships with allanite similar to the 4.5 ± 1.0 Ma-old monazite from the Kuzey detachment, a grain that is clearly extension-related. The Menderes Massif might have experienced two major stages of extension. The first occurred in the Late Oligocene, and might have affected the entire Menderes Massif. The second began in Late Miocene time and continued to present time, and might have affected only the Gordes and Central Menderes Massif. The structural and geochemical evidence and relationships between these stages of the extension, as well as their role in shaping the Cine, Gordes, and Central Menderes Massif, however, remains in question and requires further study.

Acknowledgements This paper is dedicated to Prof. Okan Tekeli who died in August 2001. The National Science Foundation (EAR-9810811 to I. Çemen) supported the project. Samples were collected by I. Çemen, O. Tekeli, and G. Seyitoglu during the summers of 1999 and 2000. The ion microprobe facility at UCLA is partly supported by a grant from the Instrumentation and Facilities Program, Division of Earth Sciences, National Science Foundation. Discussions with Y. Yilmaz, K. Gessner, M. Yazman, and M. Kohn were very helpful. We thank C. Burchfiel and J. Bartley for detailed reviews that improved the manuscript.

References

Ashworth JR, Evirgen MM (1984) Garnet and associated minerals in the southern margin of the Menderes Massif, southwest Turkey. Geol Mag 121:323–337

Ashworth JR, Evirgen MM (1985) Plagioclase relations in pelites, central Menderes, Massif, Turkey; II, Perturbation of garnet-plagioclase geobarometers. J Metamorph Geol 3:219–229

Ayers JC, Miller C, Gorisch B, Milleman J (1999) Textural development of monazite during high-grade metamorphism: Hydrothermal growth kinetics, with implications for U,Th-Pb geochronology. Am Mineral 84:1766–1780

Bozkurt E (1996) Metamorphism of Paleozoic schists in the Southern Menderes Massif: field, petrographic, textural and microstructural evidence. Turkish J Earth Sci 5:105–121
Bozkurt E, Oberhaensli R (2001) Menderes Massif (western Turkey): structural, metamorphic and magmatic evolution: a synthesis. Int J Earth Sci 89:679–708
Bozkurt E, Satir M (1999) Age of Alpine extensional shear zone in the southern Menderes Massif and its tectonic significance, western Turkey; a Rb-Sr geochronology. EUG Terra Abstracts 4:34
Catlos EJ, Harrison TM, Kohn MJ, Grove M, Ryerson FJ, Manning CE, Upreti BN (2001) Geochronologic and thermobarometric constraints on the evolution of the Main Central Thrust, central Nepal Himalaya. J Geophys Res 106:16177–16204
Catlos EJ, Gilley LD, Harrison TM (2002) Interpretation of monazite ages obtained via in situ analysis. Chem Geol 188:193–215
Cemen I, Goncuoglu MC, Dirk K (1999) Structural evolution of the Tuzgolu Basin in Central Anatolia, Turkey. J Geol 107:693–706
Cherniak DJ, Watson EB, Grove M, Harrison TM (2004) Pb diffusion in monazite: a combined RBS/SIMS study. Geochim Cosmochim Acta 68:829–840
Cressey G, Wall F, Cressey BA (1999) Differential REE uptake by sector growth of monazite. Mineral Mag 63:813–828
Dewey JF (1988) Extensional collapse of orogens. Tectonics 7:1123–1139
DeWolf CP, Belshaw N, O'Nions RK (1993) A metamorphic history from micron-scale $^{207}Pb/^{206}Pb$ chronometry of Archean monazite. Earth Planet Sci Lett 120:207–220
Doglioni C, Gueguen E, Harabaglia P, Mongelli F (1999) On the origin of west-directed subduction zones and applications to the western Mediterranean. In: Durand B, Jolivet L, Horvath F, Seranne M (eds) The Mediterranean Basins: tertiary extension within the Alpine Orogen. Geol Soc Lond Spec Publ 156:541–561
Emre T, Sozbilir H (1997) Field evidence for metamorphic core complex, detachment faulting and accommodation faults in the Gediz and Buyuk Menderes grabens (western Turkey). Int Earth Sci Coll Aegean Reg Izmir Proc 1:73–93
Ewing RC, LuMin W (2002) Phosphates as nuclear waste forms. In: Hughes JM, Kohn M, Rakovan J (eds) Phosphates: geochemical, geobiological and materials importance. Mineral Soc Am Rev Mineral Geochem 48:673–699
Finger F, Broska I, Roberts MP, Schermaier A (1998) Replacement of primary monazite by apatite-allanite-epidote coronas in an amphibolite facies granite gneiss from the eastern Alps. Am Mineral 83:248–258
Force ER (1997) Geology and mineral resources of the Santa Catalina Mountains, southeastern Arizona. Monograph Mineral Sci Center Mineral Res 1:1–135
Foster G, Kinny P, Vance D, Prince C, Harris N (2000) The significance of monazite U–Th–Pb age data in metamorphic assemblages; a combined study of monazite and garnet chronometry. Earth Planet Sci Lett 181:327–340
Gessner K, Ring U, Passchier CW, Johnson C, Hetzel R, Gungor T (2001) An active bivergent rolling-hinge detachment system: central Menderes metamorphic core complex in western Turkey. Geology 29:611–614
Harrison TM, McKeegan KD, Le Fort P (1995) Detection of inherited monazite in the Manaslu leucogranite by $^{207}Pb/^{232}Th$ ion microprobe dating: crystallization age and tectonic implications. Earth Planet Sci Lett 133:271–282
Harrison TM, Ryerson FJ, Le Fort P, Yin A, Lovera OM, Catlos EJ (1997) A Late Miocene–Pliocene origin for central Himalayan inverted metamorphism. Earth Planet Sci Lett 146:E1-E8
Harrison TM, Grove M, McKeegan KD, Coath CD, Lovera OM, Le Fort P (1999) Origin and emplacement of the Manaslu intrusive complex, Central Himalaya. J Petrol 40:3–19
Harrison TM, Catlos EJ, Montel J-M (2002) U–Th–Pb Dating of phosphate minerals. In: Hughes JM, Kohn M, Rakovan J (eds) Phosphates: geochemical, geobiological and materials importance. Mineral Soc Am Rev Mineral Geochem 48:523–558
Hetzel R, Reischmann T (1996) Intrusion age of Pan-African augen gneisses in the southern Menderes Massif and the age of cooling after Alpine ductile extensional metamorphism. Geol Mag 133:505–572
Hetzel R, Passchier CW, Ring U, Doram OO (1995b) Bivergent extension in orogenic belts; the Menderes Massif (southwestern Turkey). Geology 23:455–458
Hetzel R, Ring U, Akal C, Troesch M (1995a) Miocene NNE-directed extensional unroofing in the Menderes Massif, southwestern Turkey. J Geol Soc Lond 152:639–654
Hetzel R, Romer R, Candan O, Passchier CW (1998) Geology of the Bozdag area, central Menderes Massif, SW Turkey: Pan-African basement and Alpine deformation. Geol Rundsch 87:394–406
Isik V, Tekeli O (2001) Late orogenic crustal extension in the northern Menderes Massif (western Turkey): evidence for metamorphic core complex formation. Int J Earth Sci 89:757–765
Kingsbury JA, Miller CF, Wooden JL, Harrison TM (1993) Monazite paragenesis and U–Pb systematics in rocks of the eastern Mojave Desert, California, USA: implications for thermochronometry. Chemical Geol 110:147–167
Kohn MJ, Malloy MA (2004) Formation of monazite via prograde metamorphic reactions among common silicates: implications for age determinations. Geochim Comsochim Acta 68:101–113
Le Pichon X, Angelier J (1979) The Hellenic arc and trench system; a key to the neotectonic evolution of the eastern Mediterranean area. Tectonophysics 60:1–42
Le Pichon X, Angelier J (1981) The Aegean Sea. Phil Trans R Soc Lond A 300:357–372
Liou JG (1973) Synthesis and stability relations of epidote, $Ca_2Al_2FeSi_3O_{12}(OH)$. J Petrol 14:381–413
Lips ALW, Cassard D, Sozbilir H, Yilmaz H, Wijbrans JR (2001) Multistage exhumation of the Menderes Massif, western Anatolia (Turkey). Int J Earth Sci 89:781–792
Loos S, Reischmann T (1999) The evolution of the southern Menderes Massif in SW Turkey as revealed by zircon dating. J Geol Soc Lond 156:1021–1030
Meldrum A, Boatner LA, Weber WJ, Ewing RC (1998) Radiation damage in zircon and monazite. Geochim Cosmochim Acta 62:2509–2520
Meulenkamp JE, Wortel MJR, van Wamel WA, Spakman W, Hoogerduyn SE (1988) On the Hellenic subduction zone and the geodynamic evolution of Crete since the late middle Miocene. Tectonophysics 146:203–215
Montel J-M, Kornprobst J, Vielzeuf D (2000) Preservation of old U–Th–Pb ages in shielded monazite: example from Beni Bousera Hercynian kinzigites (Morocco). J Metamorph Geol 18:335–342
Neubauer F (2002) Evolution of late Neoproterozoic to early Paleozoic tectonic elements in Central and Southeast European Alpine mountain belts; review and synthesis. Tectonophysics 352:87–103
Oelsner F, Candan O, Oberhaensli R (1997) New evidence for the time of high-grade metamorphism in the Menderes massif, SW Turkey. Terra Nostra 97:A16
Okay AI (2001) Stratigraphic and metamorphic inversions in the central Menderes Massif; a new structural model. Int J Earth Sci 89:709–727
Overstreet WC (1967) The geologic occurrence of monazite. Geol Surv Prof Pap 530:1–327
Pan Y (1997) Zircon- and monazite-forming metamorphic reactions at Manitouwadge, Ontario. Can Mineral 35:105–118
Passchier CW, Trouw RAJ (1996) Microtectonics. Springer, Berlin Heidelberg New York, pp 1–304
Pyle JM, Spear FS (1999) Yttrium zoning in garnet: coupling of major and accessory phases during metamorphic reactions. Geol Mat Res 1:1–36
Regnier JL, Ring U, Passchier CW, Gessner K, Gungor T (2003) Contrasting metamorphic evolution of metasedimentary rocks from Cine and Selimiye nappes in the Anatolide belt, western Turkey. J Metamorph Geol 21:699–721

Reischmann T, Kroener A, Todt W, Duerr S, Sengor AMC (1991) Episodes of crustal growth in the Menderes Massif, W Turkey, inferred from zircon dating. EUG Terra Abstracts 3:34

Ring U, Gessner K, Gungor T, Passchier CW (1999) The Menderes massif of western Turkey and the Cycladic massif in the Aegean: do they really correlate? J Geol Soc Lond 156:3–6

Ring U, Willner AP, Lackmann W (2001) Stacking of nappes with different pressure–temperature paths; an example from the Menderes Nappes of western Turkey. Am J Sci 301:912–944

Satir M, Friedrichsen H (1986) The origin and evolution of the Menderes Massif, W-Turkey: a rubidium/strontium and oxygen isotope study. Geol Rundsch 75:703–714

Sengor AMC, Yilmaz Y (1981) Tethyan evolution of Turkey: a plate tectonic approach. Tectonophysics 75:181–241

Sengor AMC, Satir M, Akkok R (1984) Timing of tectonic events in the Menderes Massif, western Turkey: implications for tectonic evaluation and evidence for Pan-African basement in Turkey. Tectonics 3:693–707

Sengor AMC, Gorur N, Saroglu F (1985) Strike-slip faulting and related basin formation in zones of tectonic escape; Turkey as a case study. Spec Publ Soc Econ Paleo Mineral 37:227–264

Seyitoglu G, Scott BC (1992) Timing of Cenozoic extensional tectonics in western Turkey. J Geol Soc Lond 149:533–38

Seyitoglu G, Scott BC (1996) The cause of N-S extensional tectonics in western Turkey: tectonic escape vs back-arc spreading vs orogenic collapse. J Geodyn 22:145–153

Seyitoglu G, Leopold B, Scott BC (1994) Neogene palynological and isotopic age data from Gordes Basin, West Turkey. Newsl Strat 31:133–142

Seyitoglu G, Cemen I, Tekeli O (2000) Extensional folding in the Alasehir (Gediz) Graben, western Turkey. J Geol Soc Lond 157:1097–1100

Seyitoglu G, Tekeli O, Cemen I, Sen S, Isik V (2002) The role of the flexural rotation/rolling hinge model in the tectonic evolution of the Alasehir Graben, western Turkey. Geol Mag 139:15–26

Smith HA, Barreiro B (1990) Monazite U–Pb dating of staurolite grade metamorphism in pelitic schists. Contrib Mineral Petrol 105:602–615

Spear FS (1993) Metamorphic phase equilibria and pressure-temperature-time paths. Mineral Soc Am Washington DC 1–799

Stacey JS, Kramers JD (1975) Approximate of terrestrial lead isotope evolution by a two-stage model. Earth Planet Sci Lett 26:207–221

Stampfli GM (2000) Tethyan oceans. In: Bozkurt E, Winchester JA, Piper JDA (eds) Tectonics and magmatism in Turkey and the surrounding area. Geol Soc Lond Spec Publ 173:1–23

Stern RA, Berman RG (2000) Monazite U–Pb and Th–Pb geochronology by ion microprobe, with an application to in situ dating of an Archean metasedimentary rock. Chem Geol 172:113–130

Stern RA, Sanborn N (1998) Monazite U–Pb and Th–Ph geochronology by high-resolution secondary ion mass spectrometry. In: Radiogenic age and isotopic studies. Curr Res Geol Surv Canada 1998-F 11:1–18

Terry MP, Robinson P, Hamilton MA, Jercinovic MJ (2000) Monazite geochronology of UHP and HP metamorphism, deformation, and exhumation, Nordoyane, Western Gneiss Region, Norway. Am Mineral 85:1651–1664

Townsend KJ, Miller CF, D'Andrea JL, Ayers JC, Harrison TM, Coath CD (2000) Low temperature replacement of monazite in the Ireteba granite Southern Nevada: geochronological implications. Chem Geol 172:95–112

Whitney DL, Bozkurt E (2002) Metamorphic history of the southern Menderes Massif western Turkey. GSA Bull 114:829–838

Whitney DL, Dilek Y (1998a) Characterization and interpretation of P–T paths with multiple thermal peaks. In: Trealor PJ, O'Brien PJ (eds) What drives metamorphism and metamorphic reactions? Geol Soc Am Spec Publ 138:53–60

Whitney DL, Dilek Y (1998b) Metamorphism during Alpine crustal thickening and extension in Central Anatolia: the Nigde metamorphic core complex. J Petrol 39:1385–1403

Wing BA, Ferry JM, Harrison TM (2003) Prograde destruction and formation of monazite and allanite during contact and regional metamorphism of pelites; petrology and geochronology. Contrib Mineral Petrol 145:228–250

Yilmaz Y, Genc SC, Gurer F, Bozcu M, Yilmaz K, Karacik Z, Altunkaynak S, Elmas A (2000) When did the western Anatolian grabens begin to develop? In: Bozkurt E, Winchester JA, Piper JDA (eds) Tectonics and magmatism in Turkey and the surrounding area. Geol Soc Lond Spec Publ 173:353–384

Zhu XK, O'Nions RK (1999) Monazite chemical composition: some implications for monazite geochronology. Contrib Mineral Petrol 137:351–363